PAPER

MOF nanoparticles of MIL-68(Al), MIL-101(Cr) and ZIF-11 for thin film nanocomposite organic solvent nanofiltration membranes†

Carlos Echaide-Górriz, Sara Sorribas,‡ Carlos Téllez and Joaquín Coronas*

Nanoparticles (NPs) of MOFs MIL-101(Cr), MIL-68(Al) and ZIF-11 with sizes of 70, 103 and 79 nm, respectively, have been used in the development of thin film nanocomposite (TFN) membranes. Such membranes were synthesized with an ultrathin polyamide layer, in which NPs are embedded, about 100–150 nm thick on top of a polyimide P84® asymmetric support. Several important effects have been studied in the synthesis of the membranes for their application to organic solvent nanofiltration (OSN): the effect of the non-solvent bath, the chemical post-treatment, the concentration of precursors for interfacial polymerization and the polymerization time. The influence of different solvents (water, methanol, acetone and THF) and solutes (Acridine Orange, Sunset Yellow and Rose Bengal) on the OSN has also been studied. The hydrophilic character of the membrane and the solvent–membrane and solute–membrane interactions are shown to be the most important parameters affecting the performance of the composite membranes. A maximum permeance of 6.2 L m^{-2} h^{-1} bar^{-1} and a rejection above 90% was obtained from the combination of ZIF-11 and a post-treatment *via* filtration with dimethylformamide.

Introduction

Organic solvent nanofiltration (OSN) aims at separating molecules from specific organic solvents economically as well as efficiently. Nanofiltration was first applied to water treatment in several industries where the rejected molecule sizes were between those in reverse osmosis and ultrafiltration processes.[1] It is worth mentioning that OSN also performs well in organic solvent applications: *e.g.* in the production of xanthophylls, a yellow pigment obtained from corn, or in the Max-Dewax™ process developed by Exxon Mobile for solvent lubricant dewaxing.[1] However, the main drawback of OSN is that the membranes used in this process are only stable in a small range of organic solvents. In addition, OSN adds more complexity to the performance characterization, because more interactions between solvent, solute and membrane materials take place. In contrast processes such as ultrafiltration and microfiltration, which do not take place at a molecular level, are easily characterized because less interactions are considered.[1]

Chemical and Environmental Engineering Department, Instituto de Nanociencia de Aragón (INA), Universidad de Zaragoza, 50018 Zaragoza, Spain. E-mail: coronas@unizar.es

† Electronic supplementary information (ESI) available: MOF synthesis conditions and characterization by SEM, TEM, XRD, TGA and FTIR. See DOI: 10.1039/c6ra17522h

‡ Present address: School of Chemistry, The University of Manchester, Oxford Road, Manchester M13 9 PL, UK.

In some OSN processes, asymmetric membranes are used. Nevertheless, these are limited in terms of flux when certain organic solvents are fed.[1] In other cases, thin film composite membranes (TFC) are used. These membranes consist of three layers:[2] a non-woven support at the bottom, an intermediate layer, which is an asymmetric porous support, and an ultrathin film selective layer at the top of the membrane. The asymmetric porous support, first developed by Sourirajan and Loeb in 1962 for reverse osmosis applications,[3] can be made from a wide range of materials such as polyimide (PI) or polysulfone, among others.[1] Materials stable in organic solvents must be used in OSN. Polyimide supports are generally used.[4,5] The ultrathin selective layer is synthesized by the interfacial polymerization method (IP), making two monomers react on the surface of the porous support, or *via* coating.[2] With the IP method this layer is dense and usually made of polyamide (PA), as a result of a reaction between an amine and an acyl chloride, although some other materials have also been used (polyether amide or polyurea amide).[1]

In order to increase the permeate flux through the membrane without affecting the rejection, thin film nanocomposite (TFN) membranes were first developed by Jeong *et al.*[6] in 2007. Zeolite NaA was dispersed in an organic phase, so that during the formation of the PA layer the zeolite nanoparticles (NPs) were embedded inside it. The result was a high increase in the permeate flux through the new membrane while maintaining the rejection of the bare polymer membrane. In subsequent studies, other inorganic fillers such as hollow zeolite spheres,[7] functionalized TiO$_2$,[8] functionalized

multiwalled carbon nanotubes[9] and UZM-5 (ref. 10) were incorporated into TFN membranes. These studies were followed by the preparation of TFN membranes embedding metal–organic framework (MOF) NPs. In fact, Sorribas et al.[4] first developed this idea by adding MIL-101(Cr), ZIF-8, MIL-53(Al) and NH_2-MIL-53(Al) to the synthesized membrane, while Wang et al.[11] added ZIF-8 to a composite membrane in order to improve a dye removal process.

MOFs are hybrid organic–inorganic solid compounds with zeolite-like (porous) structures. These structures consist of the union of metallic clusters by organic linkers; this union gives many possible combinations between metals and organic compounds to form particles with different textural and chemical properties, usually highly porous and flexible. The main goal of incorporating MOFs into TFN membranes is to create selective cavities and paths in the thin film layer that may increase the solvent flux, maintaining the high rejection. Tunable MOF properties of interest for OSN applications are porosity, pore size and hydrophobicity. These properties have proved to be very influential in membrane performance. In particular, high porosity has been found to increase solvent permeance through the TFN membrane.[4] In contrast, MOF hydrophobicity might influence the OSN process depending on the feeding solvent. MIL-101(Cr) has been shown to be the MOF that gave the best performance, combined with a post-treatment that consisted of filtration with dimethylformamide (DMF).[4]

The present study continues to focus on the development of MOF-polymer mixed membranes for nanofiltration. Besides MIL-101(Cr),[4] MOFs are included that have never before been used in TFN membranes for OSN applications, such as ZIF-11 and MIL-68(Al). MIL-101(Cr) and MIL-68(Al) materials, both including carboxylate species, were first synthesized by Ferey et al.[12] and Barthelet et al.,[13] respectively. Nanosized imidazolate ZIF-11 was first reported by Sanchez-Lainez et al.,[14] based on the previous synthesis of ZIF-11.[15] The main objective is to find new MOFs that could improve the membrane performance in OSN applications, and to study how the prepared TFN membranes behave with organic solvents with different properties, such as ethers (THF) and ketones (acetone). Ketones have never before been used with MOF-based TFN membranes. Finally, membrane performance is evaluated with solutes of different sizes and properties (from 265 to 974 Da).

Experimental section

Synthesis of MOFs

ZIF-11 synthesis was based on a previously reported procedure for the formation of nano-sized particles of this material.[14] Analogous processes were used to synthesize MIL-101(Cr)[4,16] and MIL-68(Al),[17] which was synthesized using tetrahydrofuran as the synthesis solvent. The three synthesis and activation procedures can be found in the ESI.†

Preparation of porous PI supports

The porous PI supports were prepared from a 24% (w/w) polymer dope solution of P84® (HP polymer GmbH) in DMF (99.5%, Scharlab), stirred overnight. The solution obtained was allowed to stand until the air bubbles disappeared. The solution was then cast, using the Elcometer 4340 Automatic Film Applicator, on polypropylene non-woven 40 × 30 cm sheet supports and immediately immersed in a deionized water bath for 15 min, where the phase inversion process took place leading to the formation of the asymmetric porous support.

Once the porous supports were made, several chemical treatments were required so that stable TFC membranes could be built and used for OSN. After the initial immersion in the deionized water bath, the supports formed were submerged in an additional clean deionized water bath for 1 h. The supports were then immersed in two successive baths with isopropyl alcohol (IPA – 99.5%, Scharlab) for 1 h each to remove any remains of water and DMF. Afterwards, the first chemical treatment took place. This consisted of immersion in a bath of 120 g L^{-1} of hexanediamine (HDA – 98%, Sigma Aldrich) in IPA for 16 h to produce the cross-linking process, which enhanced the stability of the support in organic solvents. Four baths with IPA were applied to remove traces of HDA from the supports. Finally, the supports were immersed overnight in a solution with a 3 : 2 volume ratio of polyethylene glycol (PEG – synthesis grade, Scharlab): IPA. This prevented pore collapse during the formation of the ultrathin selective layer on the top of the support. The supports were then wiped with tissue paper.

Synthesis of the polyamide (PA) thin layer

The ultrathin layer was formed on the cross-linked porous PI support by interfacial polymerization. An aqueous solution with m-phenylenediamine (MPD – 99%, Sigma Aldrich) and an organic solution with trymesoil chloride (TMC – 98%, Sigma Aldrich) in hexane (extra pure, Scharlab) were prepared. The TMC and MPD reacted and formed the PA top layer on the support.

Firstly, 60 cm^2 porous PI support discs were coupled on the filter used for interfacial polymerization. 30 mL of the MPD aqueous solution was added for 2 min and the excess solution was removed using tissue paper. Next, 30 mL of the TMC organic solution was added for a certain time (indicated in Table 1) to form the ultrathin layer. Before removing the excess solution, 10 mL of hexane was added to stop the reaction. After removing the excess, 10 mL of hexane was added to remove unreacted TMC and finally 10 mL of deionized water was added to wash out the hexane. The TFC membranes formed were stored in deionized water. All the synthesis parameters are shown in Table 1.

In the case of TFN, the required MOF amount was dispersed in the organic solution (0.2% (w/w) of MOF in the organic phase) during three periods of 5 min sonication and 15 min stirring. The same process as for synthesizing a TFC membrane was then followed.

Two post-treatments were applied to the TFC and TFN membranes. The first consisted of washing in a 50 mL bath of DMF for 10 min at 20 °C, while the second was filtration with DMF for 10 min at a pressure of 20 bar at 25 °C. The DMF filtration was applied after 30 min of OSN with a membrane that had already undergone the DMF bath post-treatment. The post-

Table 1 Parameters when studying synthesis effects. Code legend: M TMC concentration/MPD concentration/polymerization time/non-solvent bath/post-treatment/MOF

Effect	TMC (wt%)	MPD (wt%)	Time (min)	Water bath	MOF	Post-treatment	Code
Water bath for porous support formation	0.1	2	1	Tap water	—	—	M0.1/2/1/Tap
	0.1		1	Deionized water	—	—	M0.1/2/1/De
Post-treatment	0.1	2	1	Deionized water	—	—	M0.1/2/1/De
			1		—	DMF bath	M0.1/2/1/De/b
			1		—	DMF filtration	M0.1/2/1/De/f
TMC concentration and polymerization time	0.1	2	1	Deionized water	—	—	M0.1/2/1/De
			1		—	DMF filtration	
	0.2	2	2	Deionized water	—	—	M0.2/2/2/De
			2		—	DMF filtration	
MOFs	0.1	2	1	Deionized water	—	Both	M0.1/2/1/De
					MIL-101(Cr)	(DMF bath and filtration)	M0.1/2/1/De/ M101
					MIL-68(Al)		M0.1/2/1/De/ M68
					ZIF-11		M0.1/2/1/De/f/ Z11

treatments used in this research work had previously been used by Sorribas *et al.*[4] and Solomon *et al.*[18] among others.

Several effects influencing the synthesis of the OSN membranes were studied: the effect of the water bath where the phase inversion for the preparation of the P84® support took place, the effect of the concentration of the TMC, the effect of the two post-treatments described above and the effect of the MOFs embedded inside the PA layer. In every case, at least two membranes were synthesized and tested under the same conditions of pressure and temperature (20 bar and 25 °C).

Characterization

SEM was required to observe the surfaces and cross section areas of the TFC membranes, TFN membranes, P84® porous supports and MOF morphologies, as well as to obtain particle size estimations. The presence of polyamide and MOF in the TFC and TFN membranes can be verified by observing the surface, while the presence of asymmetric pores in the support can be observed by analyzing the cross section area. A FEI-Inspect F20 microscope was used at an acceleration voltage between 10 and 20 kV with a spots of 2.5 and 3.5 nm.

Transmission electron microscopy (TEM) was useful to complement the SEM characterization, achieving more accurate particle size values. A FEI Tecnai T20 transmission electron microscope was required to conduct the analysis, using an acceleration voltage of 30 kV.

FTIR – ATR (Fourier Transform Infrared Spectroscopy – Attenuated Total Reflection) was used to study the molecular interactions that exist between the MOF nanocrystals and polyamide, and between the polyamide and polyimide, and to observe the chemical changes that occur after the post-treatments. To detect the presence of the MOFs in the thin film, the spectrum of the TFC membrane was subtracted from the spectra of the TFN membranes. A Bruker Vertex 70 Spectrophotometer with a DTGS detector and diamond ATR Golden

Gate was used. The wavenumber range measured in every case was between 500 and 4500 cm^{-1} with a resolution of 4 cm^{-1}. Thermogravimetric analysis (TGA) was used to study the thermal stability of the MOFs, as well as to find out whether they were properly activated. The measurements were taken in a Mettler Toledo TGA/SDTA 851e System, using air and a heating rate of 10 °C min^{-1}, until 850 °C.

The crystallinity of the MOFs was characterized by X-ray diffraction analysis (XRD). The equipment used was a D-Max 2500 Rigaku diffractometer with a Cu Kα ($\lambda = 0.1542$ nm) rotating anode, from 4 to 40° (2θ) with a 0.025°·s^{-1} step, operated at 40 kV and 80 mA at a wavelength of 1.5418 Å. Besides, for characterization purposes, non-supported IP was carried out without P84® and in presence of both MIL-101(Cr) and MIL-68(Al). The formation of the PA took place at the same conditions described above, but in this case both solutions (organic and aqueous with TMC and MPD, respectively) were mixed together under continuous stirring. In addition, the concentration of MOF in the organic solution was doubled (0.4% instead of the 0.2%) to favor the detection of MOFs by the diffractometer. This characterization allowed to investigate if the IP affected the crystallinity of the MOFs. In this case, the same diffractometer was used, although the range of 2θ analyzed was 5–12°. This is the interval where the main MIL-101(Cr) and MIL-68(Al) intensities appear.

Nitrogen adsorption analysis was used to obtain the MIL-101(Cr) and MIL-68(Al) specific surface areas, calculated by the Brunauer–Emmett–Teller (BET) method. The experiments took place at 77 K under variable relative pressure. The equipment used was a Micrometrics Tristar 3000. Degasification before the nitrogen adsorption experiment took place at 200 °C for 8 h. The pore volume was calculated with the adsorbed volume at a relative pressure near to saturation (0.98).

The hydrophilicity/hydrophobicity of the formed TFN membranes was characterized by contact angle measurements at up to three different places in every membrane sample. The Krüss

DSA 10 MK2 equipment used for this purpose measures the contact angle by dropping water on the surface of the membrane.

XPS experiments were conducted to detect and quantify the presence of metals that form part of the MOFs added to the membranes. The content of MOF in a given membrane was obtained by relating the quantity of metal in the MOF through its empirical equation. Considering the relation between the metal and the whole MOF, the quantity of MOF in a membrane can be estimated. XPS characterization was performed with a Kratos Axis Ultra spectrometer employing a monochromatic Al Kα (1486.6 eV) X-ray source at 10 mA and 15 kV and a power of 150 W. The samples were first evacuated at room temperature (pressures near 10^{-11} bar were observed during surface analysis) and analyzed in 0.11×0.11 mm^2 areas under the same conditions.

OSN

The OSN process was carried out in a dead-end membrane module (Sterlitech HP4750), where a feed of 20 mg L^{-1} of a dye in methanol was pushed to permeate through a membrane with constant stirring. The effective area of the membrane was 12 cm^2 and the feed volume was 250 mL (the total capacity of the module was 300 mL and the maximum operating pressure 69 bar). The rejection and permeate flux were calculated using the following equations:

$$Q = \frac{V}{A \times t} = \left[\frac{L}{m^2 \times h}\right] \tag{1}$$

$$\text{Permeance} = \frac{Q}{\Delta P} = \left[\frac{L}{m^2 \times h \times \text{bar}}\right] \tag{2}$$

$$\text{Rejection (\%)} = \left(1 - \frac{C_{\text{permeate}}}{C_{\text{residue}}}\right) \times 100 \tag{3}$$

where V represents the volume (L), A the membrane nano-filtration area (cm^2), t the time for permeate collection (h), and ΔP the pressure drop through the membrane (bar). Concentrations of permeate (C_{permeate}) and residue (C_{residue}) were both measured by an UV spectrometer (Jasco V-670 spectrophotometer) using water as solvent. For this purpose, after 30 min, which is the time the process needs to stabilize, 3 mL of each permeate and residue were taken as samples for analysis. The methanol in the samples was allowed to evaporate and was replaced by 3 mL of deionized water at ambient temperature and pressure to be measured with the UV spectrometer. Absorbance and concentration values for each solute used were related by an equation obtained from the calibration.

The wavelengths of maximum absorbance of Rose Bengal (RB – Sigma-Aldrich, 95% dye content), Sunset Yellow (SY – Sigma-Aldrich, 90% dye content) and Acridine Orange (AO – Acros Organics, 55% dye content) were 546 nm, 480 nm and 291 nm, respectively.

Results and discussion

MOFs characterization

SEM and TEM showed similar crystal morphologies to those described in the literature for each MOF (see Fig. S1 and S2 from the ESI†)[14,16,17] as well as adequate average particle sizes of 70 ± 6 and 79 ± 10 nm for MIL-101(Cr) and ZIF-11, respectively, and 103 ± 15 nm for MIL-68 (Al) (see Table 2). The MIL-101(Cr) and MIL-68(Al) crystalline structures were confirmed by XRD analysis (Fig. S3A and S3B from the ESI†). It is worth mentioning that the nanosized ZIF-11 was not crystalline like typical microsized crystals, as the XRD analysis showed (Fig. S3C from the ESI†); however, most of the chemical and adsorption features of ZIF-11 can also be found in the nanosized ZIF-11.[14] TGA (Fig. S4 from the ESI†) and nitrogen adsorption analyses indicated that the solvent and unreacted linkers were washed out after the whole synthesis process, *i.e.* the MOF nanoparticles were correctly activated. Table 2 shows the BET specific surface areas (2597 and 1394 m^2 g^{-1} for MIL-101(Cr) and MIL-68(Al), respectively) obtained by the BET method and the pore volumes. The specific surface area of the ZIF-11 could not be measured by nitrogen adsorption, since its pores are smaller than the nitrogen kinetic diameter.

Effect of support on OSN performance

Obvious differences were encountered when the PI support was synthesized in tap water (hardness about 25 °fH due to the presence of calcium and magnesium salts, °fH corresponding to French degrees of hardness, defined as 10 mg L^{-1} CaCO$_3$) and deionized water. When a tap water bath was used as a non-solvent in the phase inversion process, the support obtained did not correspond to the expected asymmetric porous support with evident finger-like macropores along the cross section (Fig. 1A). In fact, this cross section revealed a homogeneous texture, which contrasts with that of a support whose phase inversion took place with deionized water as the non-solvent (Fig. 1B, with evident finger-type macropores). In addition, the surface of the non-asymmetric support (Fig. 1C) seems to be formed by larger pores than the asymmetric one (Fig. 1D). These differences had already been found in research conducted by Yang and Liu,[19] who studied the effect of salts dissolved in a non-solvent during the phase inversion. As they demonstrated, the diffusion rate of the non-solvent as well as the driving force through the polymer dope solution cast decreased with the salt concentration. This effect might have slowed down the polymer precipitation, leading to a homogeneous pore size distribution.

The differences described between both types of support have a strong effect on the OSN performance. The sub-layer finger type appearance with a denser layer on top as seen in Fig. 1B above is consistent with the lower transport resistance of the PI P84® support. In agreement with this, the permeance was higher when the TFC membrane was obtained with a porous support prepared with tap water as a non-solvent than when using deionized water (3.0 and 1.5 L m^{-2} h^{-1} bar^{-1}, respectively). Moreover, membranes made from supports prepared in tap and deionized baths showed differences in Sunset Yellow (SY) rejection: 51.7% and 87.0%, respectively (see Fig. 2A). In conclusion, the membrane made from a support prepared in tap water was more permeable but less selective. The morphologies described above and the results obtained in the

Table 2 Particle size and textural properties of MOFs

MOF	Size[a] (nm)	Specific surface ($m^2\ g^{-1}$)	Pore volume ($cm^3\ g^{-1}$)	Pore diameter (nm)	Cavities (nm)
MIL-101(Cr)	70 ± 6	2597 ± 31	1.8	1.2–1.6 (ref. 16)	2.9–3.4 (ref. 16)
MIL-68(Al)	103 ± 15	1394 ± 23	1.1	0.6–0.64 and 1.6–1.7 (ref. 17)	—
ZIF-11	79 ± 10	—	0.11[b]	0.3 (ref. 14)	1.46 (ref. 14)

[a] Values correspond to the average of particles measured in SEM images. [b] Pore volume for ZIF-11 was obtained by carbon dioxide adsorption at 0 °C and using the Dubinin–Radushkevich equation to the low pressure region.[14]
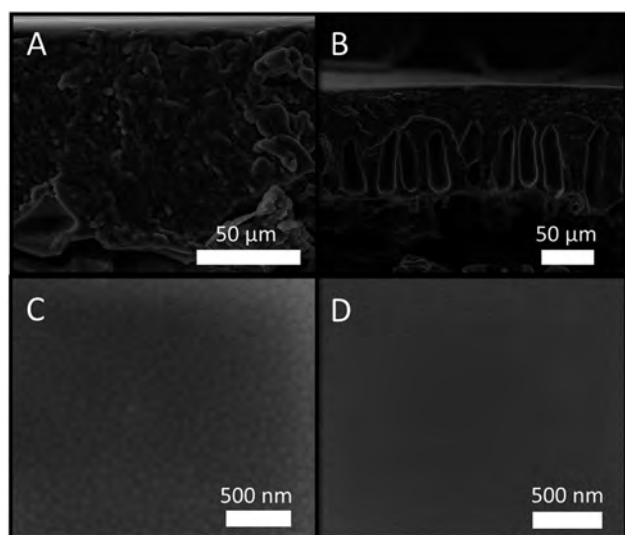
Fig. 1 SEM images of the cross section of a P84® support prepared with deionized water (B) and with tap water (A). SEM images of the surface area of the same support prepared with tap water (C) and deionized (D).

OSN suggest that when the interfacial polymerization was carried out, the amine was not retained inside the superficial pores of the support synthesized with tap water as the non-solvent liquid. In other words, its surface was not dense enough to act as a reservoir for the MPD. Therefore, when the organic phase was in contact with the surface of the support in order to let the interfacial polymerization occur, the PA thin film was not able to be formed continuously and homogeneously and the results obtained were less reproducible (larger error bar in Fig. 2A). Hereafter, all the reported membranes were prepared using deionized water as a non-solvent.

Effect of post-treatment on OSN

The results obtained in this study show the same tendency as those reported by Sorribas et al.[4] Both bath and filtration DMF post-treatments improved the OSN performance of TFC membranes. The highest permeance and rejection were obtained when the DMF filtration post-treatment was applied. When the DMF bath was used, the permeance increased from 1.5 to 2.8 L $m^{-2}\ h^{-1}\ bar^{-1}$, while with DMF filtration the increase was from 1.5 to 3.8 L $m^{-2}\ h^{-1}\ bar^{-1}$ (see Fig. 2B). Analogously, the rejection increased from 87.0 to 90.3% and

from 87.0 to 95.7% when DMF bath and filtration were carried out, respectively (see Fig. 2B).

The increase in permeance can be explained in terms of Hansen solubility parameters (HSP).[20,21] These parameters are δ_D, δ_P and δ_H for dispersion or London interaction, polar interaction and hydrogen bonds, respectively. The similarity between PA and DMF HSP, obtained calculating the parameter Ra (see Table 5), means that the solvent may dissolve low molecular mass fragments of PA, as Solomon et al.[18] reported. Consequently, the resistance to mass transport through the membrane decreased, and the permeate flux increased. This effect occurred mostly at the surface of the membrane when a DMF bath post-treatment was applied, but intensified through the entire membrane thickness with DMF filtration.

The increase in rejection, on the other hand, was due to the contribution of three different effects. Firstly, a swelling effect provoked in the membrane when contacts with DMF, leading to a compression effect that tends to remove imperfections and defects in the top layer.[18] Secondly, a process of surface defect healing by surface tension driven pore collapse, as reported by Mukherjee et al.[22] Finally, dissolved PA monomers during the DMF filtration treatment, with minimum molecular mass of up to 271 g mol^{-1},[23] rejected by the PA thin film might heal small defects in the selective film.

Effect of concentration of TMC and polymerization time on OSN

The results obtained show differences in permeance and rejection when the TMC concentration as well as the polymerization time were doubled and no post-treatment was applied, although slight changes were observed when DMF filtration post-treatment was carried out (see Fig. 2C).

The effect of the TMC concentration in membranes with no post-treatment applied follows the same tendency as that previously observed by Ahmad and Ooi,[24] who showed how pore size and thin film effective thickness decreased when the TMC concentration increased with a constant MPD concentration.

Furthermore, Chai and Krantz[25] studied the formation of the PA concluding that the TMC concentration influenced the reaction mechanism when the MPD concentration was constant. They observed that the TMC diffusion controlled the process when its concentration was low (below 0.02%), and that the MPD diffusion through the formed PA film controlled the process when the TMC concentration was high (above 0.02%).
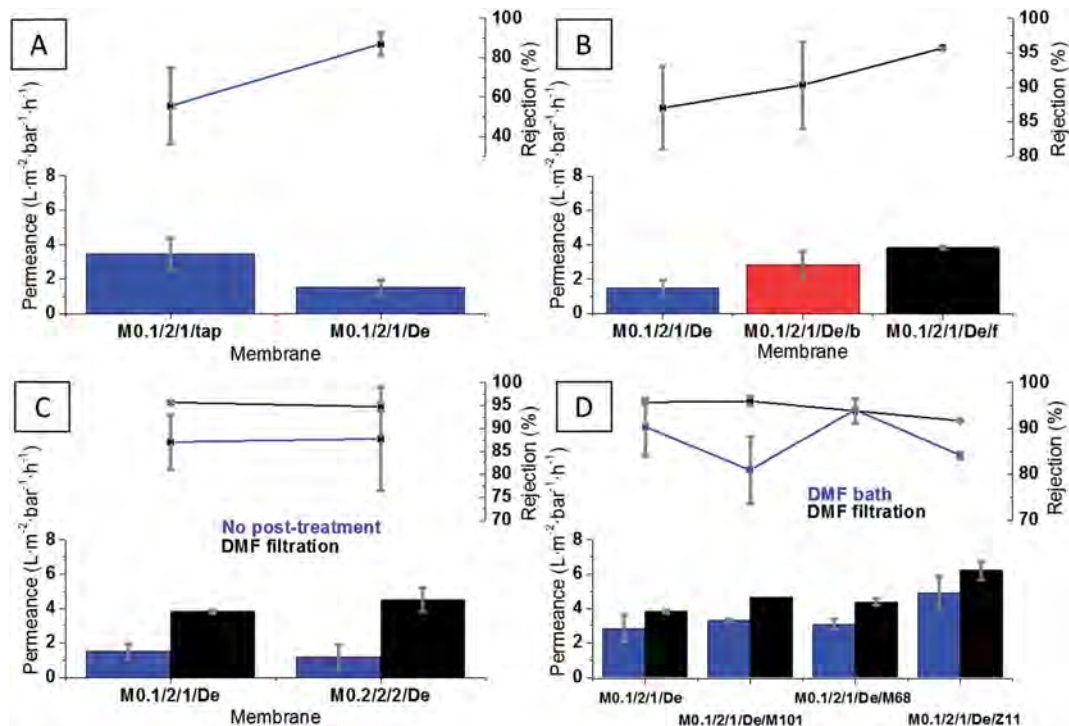
Fig. 2   OSN performance effect of: support (A) M0.1/2/1/tap (TFC membrane synthesized with a support using tap water as non-solvent) and M0.1/2/1/De (TFC membrane with a support made using deionized water as non-solvent); post-treatment (B) M0.1/2/1/De (with no post-treatment), M0.1/2/1/De/b (with DMF bath as post-treatment) and M0.1/2/1/De/f (with DMF filtration as post-treatment); TMC concentration (C) M0.1/2/1/De and M0.2/2/2/De (TMC concentration and polymerization time doubled) and type of MOF (D). In all cases SY (452 Da) in methanol was filtered.

In contrast, the influence of the MPD concentration on the reaction mechanism for a given TMC concentration is mostly focused on the orientation of the PA thin film growth. This effect becomes very clear when the MPD concentration is low (0.02%): the TMC diffusion rate is higher than that of the MPD, so the first monomer diffuses faster than the second through the PA thin layer, and therefore the thin film grows towards the aqueous phase. Chai and Krantz[25] also observed that high TMC concentrations can benefit the film cross-linking, making the process self-controlled. This is of interest because the thin film thickness will not depend on the reaction time beyond a certain time. Finally, the MPD concentration can also influence cross-linking and, although Chai and Krantz[25] observed that the thin film thickness is not affected by MPD concentration, it could affect the membrane stability and solute rejection when filtering organic solvents.

Nevertheless, as mentioned before, DMF post-treatment tends to equalize membrane performance in OSN regardless of the TMC concentration. According to these results, high concentrations of TMC and MPD are required, in agreement with Chai and Krantz[25] However, higher TMC concentrations gave rise to worse membrane performances and higher deviation in rejection when no post-treatment was carried out as well as less rejection when DMF filtration was applied, as Fig. 2C shows, thus the best synthesis conditions, chosen for the remaining study, were 0.1 wt% of TMC with 1 min of interfacial polymerization.

Membrane characterization

The SEM results show the presence of PA on the top of the TFC membranes (Fig. 3A), which forms ring-like structures over the flat surface of the porous support. These structures also appeared in TFN membranes, synthesized in the presence of MOFs MIL-68(Al), MIL-101(Cr) and ZIF-11 (Fig. 3B–D, respectively), thus the corresponding top selective PA layers seem to be formed. As reported in the literature,[26] during interfacial polymerization PA tends to wrap every single particle, even those which may have some agglomeration. The presence of MOFs in the membrane surface (about 10 nm deep) was also confirmed by XPS characterization (Table 3). MOF contents in the top PA thin film were estimated to be 11.4, 17.5 and 0.9 wt% in case of MIL-101(Cr), MIL-68(Al) and ZIF-11, respectively. The low amount of ZIF-11 detected by XPS suggests a filler distribution mostly inside the PA layer and somewhat below the surface.[26,27]

Regarding FTIR-ATR, characterization peaks at 1642 and 1532 cm^{-1} in a porous P84® support corresponded to C=O stretching and C–N stretching, respectively (see the peaks highlighted in purple in Fig. S5A from the ESI†). Both bonds were formed by the cross-linking treatment. The peak at 1090 cm^{-1}, which corresponds to a C–H stretching bond, belongs to the PEG ether group (see the peaks highlighted in light green in Fig. S5A from the ESI†).[4] PEG disappeared after interfacial polymerization, so its peak does not appear in the FTIR-ATR spectrum of the forming TFC. These results are evidence of
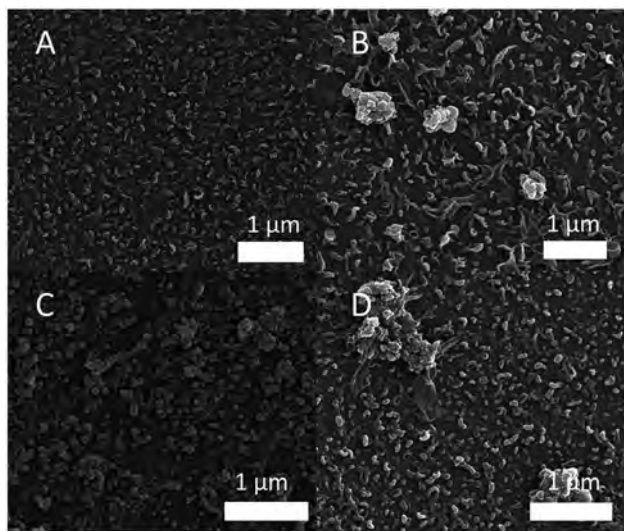
Fig. 3 SEM of TFC membrane (A) of TFN – MIL-68(Al) (B), of TFN – MIL-101(Cr) (C) and of TFN – ZIF-11 (D).

the two chemical treatments applied during the porous support preparation. When TFN membranes were analyzed, some new peaks appeared due to the presence of MOFs in the selective thin layer. MIL-101(Cr) and MIL-68(Al) TFN membranes exhibit a peak at 1413 cm^{-1} (more clearly after subtraction of the TFC membrane spectrum, see Fig. S5B from the ESI†) due to the presence of linker COO^{-} groups.[4,17] Other intensities corresponding to the MOFs did not appear in the TFN spectra because the concentration of crystals in the PA thin film is too low to be detected by FTIR. Finally, no intensities could be identified from the membrane containing ZIF-11 (especially its highest intensity at around 750 cm^{-1}, see Fig. S5D from the ESI†), probably due to the low MOF concentration in the PA thin film.

Regarding the XRD characterization of MOF-PA composites similar in composition to TFN membranes, the main intensities of both MIL-101(Cr) and MIL-68(Al) are present in the corresponding XRD patterns (see Fig. S6 from the ESI†). This allows to infer that the IP did not alter the crystallinity of the MOFs. The ZIF-11 PA composite was not analyzed due to the lack of crystallinity of this MOF as said above (see Fig. S3C from the ESI†).

Effect of MOFs on OSN

As shown in Fig. 2D, the addition of ZIF-11 and MIL-101(Cr) to TFC membranes increased their permeance; however, that of

MIL-68(Al) generated a slight change in the OSN performance. In every case, the effect of the post-treatment was observed. In both Fig. 2B and D, it can be seen that the permeances and corresponding rejections followed the same trends when the two different post-treatments were applied. The best performances were obtained when the DMF filtration post-treatment was applied: over 90% of rejection and the highest permeances (3.8 to 6.2 L m^{-2} h^{-1} bar^{-1}) for each TFN membrane. The highest permeance (6.2 L m^{-2} h^{-1} bar^{-1}) was obtained by using a TFN membrane synthesized with ZIF-11 and treated with DMF filtration. Since Sorribas et al. reported that 0.2% of MOF in the hexane solution gave rise to the best results,[4] this determines the best parameters of the membrane synthesis according to the effects studied.

As previously reported,[4] the MIL-101(Cr) increases the methanol permeance due to its intrinsic high porosity; mainly determined by the specific surface area and porous volume (see Table 2). Methanol molecules can permeate through either the MOF pores because of its small size (see Table 5) below that of the MIL-101(Cr) pore size (see Table 2), or through spaces between MOF particles when small agglomerates are present in the TFN membrane. Transport mechanism of methanol through the hollow spaces created by MOF MIL-68(Al) should be similar to that through MIL-101(Cr) because the textural properties of both MOFs are not so different (see Table 2). In the case of both MILs, the transport mechanism of methanol through bare PA areas corresponds to the so-called solution-diffusion mechanism, but the transport mechanism through the MOFs is based on diffusion through their pores. On the contrary, methanol molecules cannot diffuse through the ZIF-11 pores because the methanol kinetic diameter (see Table 5) is above the pore diameter of this MOF (see Table 2). Consequently, the effect of ZIF-11 on the TFN membrane transport is justified based on the chemical interactions that influence the structure of the PA thin film, changing the PA cross-linking. This hypothesis was already postulated by Duan et al.,[26] who tested different concentrations of ZIF-8 on TFN membranes and concluded that ZIF-8 decreased the degree of cross-linking in the PA thin film. When the cross-linking decreases, the solvent permeance increases, but the solute rejection may diminish.[26] Besides, the creation of voids in the ZIF-11 PA interfaces cannot be ruled out, which would increase the solvent permeance, even though high compatibility between MOFs and polymers have been reported.[4] Finally, the formation of small agglomerations of ZIF-11 (embedded in PA) may create selective spaces between particles, some of them large enough to allow the solvent permeate through them.

Table 3 Atomic compositions of elements in TFN membranes by XPS. Average and standard deviation values were obtained from measurements in two different sample areas

	%Metal	%C	%O	%N	MOF[a] (wt%)
TFN-MIL101(Cr)	1.3 ± 0.0	71.9 ± 0.0	18.8 ± 0.0	8.0 ± 0.0	11.4 ± 0.0
TFN-MIL68(Al)	2.1 ± 0.0	70.0 ± 0.0	18.3 ± 0.0	9.6 ± 0.0	17.5 ± 0.0
TFN-ZIF11(Zn)	0.1 ± 0.0	73.8 ± 0.0	16.2 ± 0.0	9.8 ± 0.0	0.9 ± 0.0

[a] MOF contents were estimated from composition of metals as reference.

Table 4 Contact angle measurements

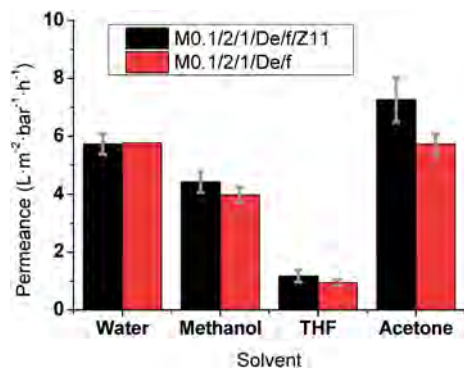| Membranes	Contact angle (°)
TFC	71 ± 2
TFN ZIF-11	72 ± 3
TFN MIL-101	57 ± 4
TFN MIL-68	60 ± 3

Fig. 4 Effect of pure solvent in OSN using TFC membrane (red) and TFN membrane with ZIF-11 (black), both with DMF filtration post-treatment applied.

As Sorribas *et al.* proved,[4] in the TFN membrane, the PA thin film grows on the nanoparticles, so these are completely coated by the polymer. Since it was already demonstrated that the PA formation is limited by the transport of the monomers during the interfacial polymerization,[25] the film formed on the nanoparticle keeps the same thickness as the PA thin film grown in a TFC membrane. Consequently, the nanoparticles increase the effective area showed by the membrane, increasing the solvent permeance.

Using ZIF-11 as a filler, the permeation increased when the nanoparticles were added because better MOF-polymer interaction was achieved, probably due to the hydrophobic character of ZIF-11. This hydrophobic character of ZIF-11, as compared to MIL-101(Cr) and MIL-68(Al), was evidenced by contact angle measurements (see Table 4). In consequence, hydrophilic carboxylate based MIL-101(Cr) and MIL-68(Al) interact more strongly with polar methanol molecules than ZIF-11, thus their flows tend to decrease as compared to composite membranes synthesized with ZIF-11. Sorribas *et al.*[4] observed this effect comparing membrane performance when filtering THF and methanol. Nevertheless, the permeance when using MIL-101(Cr) was still high because of the high porosity of this MOF; although its hydrophilic character slowed down methanol transport, which is based on MOF pore diffusion.

Effect of solvents

A TFC membrane and a TFN membrane synthesized with ZIF-11 were tested with four different pure solvents (no solute): water, methanol, THF and acetone. As can be seen in Fig. 4, the solvent permeances through both membranes follow the same pattern: acetone > water > methanol > THF. The permeances were higher with ZIF-11-TFN than with TFC membranes. The same membrane was used in each case to filtrate the four solvents (first water, second methanol, third THF and finally acetone).

The differences in permeances may be explained by a combination of factors such as the solvent polarity (it is important to remember that ZIF-11 enhances the hydrophobicity of TFC membranes, as the contact angle measurements revealed), the solvent-selective layer polymer (PA) interactions (estimated by HSP comparison) and the kinetic diameters of the solvent (see Table 5). According to the relative permittivity values, THF is likely to be the least polar solvent of the four used. However, the THF flow is the lowest of all of them. This unexpected result is explained by its kinetic diameter (which is the highest) and by the low interaction between the solvent and the selective PA layer, according to the HSP calculation for both of them (the lower the Ra value calculated, the better the solubility, *i.e.* the interaction). On the other hand, the acetone flow is the highest in both membranes, which is explained by the weak polarity of the molecule, the small kinetic diameter (in relation to the rest of the solvents) and the significant interaction with PA. High permeances were obtained for methanol and water because of their small kinetic diameters, in spite of their low interaction with PA in terms of HSP.

The effect of the presence of ZIF-11 in the membrane was likely to be the strongest with acetone, although it was relevant with THF and methanol. However, when water was fed the permeance with or without ZIF-11 tended to remain unchanged. The hydrophobic character enhanced by the presence of the

Table 5 Solvent properties. Relative permittivity, related to molecule polarity. Hansen parameter differences (Ra) calculated as described in Hansen,[29] obtained by using HSP of each solvent and PA

Solvent	Relative permittivity[30]	Kinetic diameters[31–33] (Å)	δ_D (MPa$^{0.5}$)	δ_P (MPa$^{0.5}$)	δ_H (MPa$^{0.5}$)	Ra – solvent/PA[a] (MPa$^{0.5}$)
Methanol	33.0	3.6	15.1	12.3	22.3	15.5
DMF	38.2	5.5	17.4	13.7	11.3	4.0
THF	7.5	6.3	16.8	5.7	8.0	6.6
Acetone	21.0	4.6	15.5	10.4	7.0	5.3
Water	78.4	2.7	15.5	16.0	42.3	35.0
PA	—	—	18.0	11.9	7.9	0

[a] Calculated according to $Ra^2 = 4(\delta_{D1} - \delta_{D2})^2 + (\delta_{P1} - \delta_{P2})^2 + (\delta_{H1} - \delta_{H2})^2$ where δ_{D1}, δ_{P1} and δ_{H1} and δ_{D2}, δ_{P2} and δ_{H2} are sets of parameters corresponding to PA and solvent, respectively.
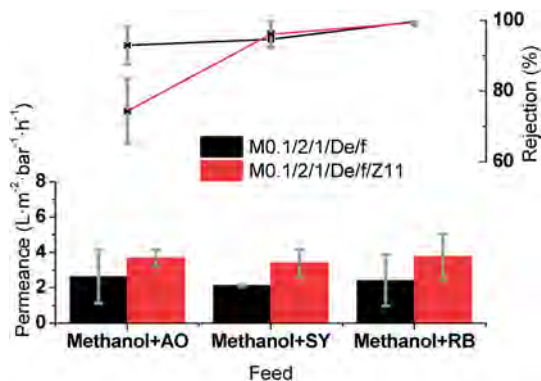
Fig. 5 Effect of solute in OSN using TFC membrane (black) and TFN membrane with ZIF-11 (red), both with DMF filtration post-treatment applied.

MOF, which made the thin film less hydrophilic, can explain this phenomenon. Yang et al.[28] explained the permeance of organic solvents by solvent-membrane interactions such as hydrogen bonding. This may also apply in this case since the permeance of solvents with lower hydrogen bonding HSP (δ_H in Table 5) increased after losing some hydrophilicity when ZIF-11 was added.

Effect of solutes

As in the previous solvent study, the membrane that showed the best performance was compared to a TFC membrane. However, in this case both membranes were fed with three consecutive solutions, starting with an Acridine Orange (AO, 265 Da)-methanol solution, followed by a SY (452 Da)-methanol and ending with a Rose Bengal (RB, 1017 Da)-methanol solution.

As can be seen in Fig. 5, the methanol permeance in both types of membranes when AO was filtered were lower than when SY was filtered in the clean membranes (Fig. 2D). These differences can be explained by two facts. Firstly, the HSP values of AO show relatively stronger interactions with bare PA and benzimidazol (bIm), which is a ZIF-11 linker (Table 6). Paseta et al.[34] discussed the interactions between ZIF-8 and caffeine by comparing the HSP of caffeine and ZIF-8 linker instead of ZIF-8 itself because of general MOF HSP unavailability. In contrast, SY interactions with both PA and bIm seem to be much weaker. This suggests that more extensive fouling taking place during the filtration process, and in consequence the methanol permeance would decrease, when filtering AO and the successive solutes. Secondly, as mentioned by Jhaveri and Murthy[35]

superficial hydrophilicity in membranes tends to decrease fouling phenomena. In this case, as ZIF-11 decreases the hydrophilic character of the membrane (Table 4), some additional tendency to fouling would be expected with this filler as compared to the bare membrane or TFN membranes containing less hydrophobic MOFs as fillers.

AO rejection became less reproducible and slightly lower than the rest of the solutes when a ZIF-11 containing membrane post-treated with DMF was tested. This could be due to an increase in the non-selective transport. Here, the effects of DMF filtration did not have the same consequences for the AO rejection as they had when SY was filtered (Fig. 2D). In other words, membrane compaction, pore collapse and redistribution of PA monomers did not heal the top selective layer of PA so as to increase AO rejection.

However, the presence of ZIF-11 has a relevant impact on methanol permeance, which was enhanced when SY and RB were filtered, according to the HSP of all the agents involved in the filtration of AO, SY and RB dissolved in methanol through a membrane synthesized with or without ZIF-11 (Table 6). The differences in solvent permeances may be caused by the interactions between AO and PA and benzimidazole (lowest Ra values in Table 6). The weaker interactions in terms of HSP when SY and RB were filtered enhanced the methanol permeance.

Conclusions

Nanofiltration permeance of methanol has been improved by adding MOFs (MIL-101(Cr), MIL-68(Al) and ZIF-11) to thin film nanocomposite (TFN) membranes and applying post-treatments such as bath and filtration of DMF. The presence of ZIF-11 clearly increased the methanol permeance, even compared to the other two MOFs tested. Besides, the presence of ZIF-11 and the application of DMF filtration produced a similar effect on all the organic solvents and solutes tested by nanofiltration. However, the methanol permeance was lower when filtering AO than when filtering SY. Interactions between the solutes and polymer as well as with the ZIF-11 linker, discussed in terms of Hansen solubility parameters (HSP), are probably responsible for the decrease in methanol permeance when filtering AO. Fouling phenomena could also contribute to the permeance decreases observed. Finally, interactions between the solute and membrane can decrease permeance, thus the same membrane did not exhibit the same behavior when the solute was changed.

Table 6   HSP of solutes, PA and benzimidazole (bIm)

	δ_D (MPa$^{0.5}$)	δ_P (MPa$^{0.5}$)	δ_H (MPa$^{0.5}$)	Ra (solute/PA – MPa$^{0.5}$)	Ra (solute/benzimidazole – MPa$^{0.5}$)
AO	20.2	3.2	6.4	9.9	12.6
SY	23.1	17.8	24.1	20.0	14.3
RB	25.1	3.6	9.7	16.5	14.5
Aromatic PA	18.0	11.9	7.9	0	—
Benzimidazole	20.6	14.9	11.0	—	0

The results obtained show that besides the importance of MOF porosity in OSN permeance with TFN membranes, the modification of the membrane hydrophilicity can also play an important role. This effect was observed when the four different solvents (water, methanol, acetone and THF) were tested since different results were obtained with TFC membranes and TFN membranes synthesized with ZIF-11. The solvent permeances through both membranes are in the following order: acetone > water > methanol > THF. The permeances were higher with the ZIF-11 TFN than with the TFC membranes. In addition, the hydrophilicity effect was combined with interactions explained by the HSP and the kinetic diameter values of the molecules.

Acknowledgements

Notes and references

1 P. Vandezande, L. E. M. Gevers and I. F. J. Vankelecom, *Chem. Soc. Rev.*, 2008, **37**, 365–405.
2 S. Hermans, H. Marien, C. Van Goethem and I. F. J. Vankelecom, *Curr. Opin. Chem. Eng.*, 2015, **8**, 45–54.
3 S. Loeb and S. Sourirajan, *Adv. Chem.*, 1963, **38**, 117–132.
4 S. Sorribas, P. Gorgojo, C. Tellez, J. Coronas and A. G. Livingston, *J. Am. Chem. Soc.*, 2013, **135**, 15201–15208.
5 S. Hermans, E. Dom, H. Marien, G. Koeckelberghs and I. F. J. Vankelecom, *J. Membr. Sci.*, 2015, **476**, 356–363.
6 B. H. Jeong, E. M. V. Hoek, Y. S. Yan, A. Subramani, X. F. Huang, G. Hurwitz, A. K. Ghosh and A. Jawor, *J. Membr. Sci.*, 2007, **294**, 1–7.
7 K. Vanherck, A. Aerts, J. Martens and I. Vankelecom, *Chem. Commun.*, 2010, **46**, 2492–2494.
8 M. Peyravi, M. Jahanshahi, A. Rahimpour, A. Javadi and S. Hajavi, *Chem. Eng. J.*, 2014, **241**, 155–166.
9 S. Roy, S. A. Ntim, S. Mitra and K. K. Sirkar, *J. Membr. Sci.*, 2011, **375**, 81–87.
10 M. Namvar-Mahboub, M. Pakizeh and S. Davari, *J. Membr. Sci.*, 2014, **459**, 22–32.
11 L. Y. Wang, M. Q. Fang, J. Liu, J. He, L. H. Deng, J. D. Lib and J. D. Lei, *RSC Adv.*, 2015, **5**, 50942–50954.

12 G. Ferey, C. Mellot-Draznieks, C. Serre, F. Millange, J. Dutour, S. Surble and I. Margiolaki, *Science*, 2005, **309**, 2040–2042.
13 K. Barthelet, J. Marrot, G. Ferey and D. Riou, *Chem. Commun.*, 2004, 520–521.
14 J. Sanchez-Lainez, B. Zornoza, A. Mayoral, A. Berenguer-Murcia, D. Cazorla-Amoros, C. Tellez and J. Coronas, *J. Mater. Chem. A*, 2015, **3**, 6549–6556.
15 K. S. Park, Z. Ni, A. P. Cote, J. Y. Choi, R. D. Huang, F. J. Uribe-Romo, H. K. Chae, M. O'Keeffe and O. M. Yaghi, *Proc. Natl. Acad. Sci. U. S. A.*, 2006, **103**, 10186–10191.
16 N. A. Khan, I. J. Kang, H. Y. Seok and S. H. Jhung, *Chem. Eng. J.*, 2011, **166**, 1152–1157.
17 B. Seoane, V. Sebastian, C. Tellez and J. Coronas, *CrystEngComm*, 2013, **15**, 9483–9490.
18 M. F. J. Solomon, Y. Bhole and A. G. Livingston, *J. Membr. Sci.*, 2012, **423**, 371–382.
19 S. Yang and Z. Z. Liu, *J. Membr. Sci.*, 2003, **222**, 87–98.
20 C. M. Hansen, *Prog. Org. Coat.*, 2004, **51**, 77–84.
21 C. M. Hansen, *Eur. Polym. J.*, 2008, **44**, 2741–2748.
22 D. Mukherjee, A. Kulkarni and W. N. Gill, *Desalination*, 1996, **104**, 239–249.
23 W. J. Lau, A. F. Ismail, N. Misdan and M. A. Kassim, *Desalination*, 2012, **287**, 190–199.
24 A. L. Ahmad and B. S. Ooi, *J. Membr. Sci.*, 2005, **255**, 67–77.
25 G. Y. Chai and W. B. Krantz, *J. Membr. Sci.*, 1994, **93**, 175–192.
26 J. T. Duan, Y. C. Pan, F. Pacheco, E. Litwiller, Z. P. Lai and I. Pinnau, *J. Membr. Sci.*, 2015, **476**, 303–310.
27 M. L. Lind, A. K. Ghosh, A. Jawor, X. F. Huang, W. Hou, Y. Yang and E. M. V. Hoek, *Langmuir*, 2009, **25**, 10139–10145.
28 X. J. Yang, A. G. Livingston and L. F. dos Santos, *J. Membr. Sci.*, 2001, **190**, 45–55.
29 C. M. Hansen, *Hansen Solubility Parameters: A User's Handbook*, CRC Press, Boca Raton, 2nd edn, 2007.
30 *Lange's Handbook of Chemistry*, ed. J. G. Speight, McGraw-Hill, New York, 16th edn, 2005.
31 T. Borjigin, F. X. Sun, J. L. Zhang, K. Cai, H. Ren and G. S. Zhu, *Chem. Commun.*, 2012, **48**, 7613–7615.
32 J. Y. Lee, T. S. Yun, J. C. Santamarina and C. Ruppel, *Geochem., Geophys., Geosyst.*, 2007, **8**, 10.
33 T. Kajiwara, M. Higuchi, A. Yuasa, H. Higashimura and S. Kitagawa, *Chem. Commun.*, 2013, **49**, 10459–10461.
34 L. Paseta, G. Potier, S. Abbott and J. Coronas, *Org. Biomol. Chem.*, 2015, **13**, 1724–1731.
35 J. H. Jhaveri and Z. V. P. Murthy, *Desalination*, 2016, **379**, 137–154.